Molecular conformation of a peptide fragment of transthyretin in an amyloid fibril

Christopher P. Jaroniec*, Cait E. MacPhee†‡, Nathan S. Astrof*, Christopher M. Dobson§, and Robert G. Griffin*‡

*Department of Chemistry and Center for Magnetic Resonance, Francis Bitter Magnet Laboratory, Massachusetts Institute of Technology, Cambridge, MA 02139; †Cavendish Laboratory, University of Cambridge, Madingley Road, Cambridge CB3 0HE, United Kingdom; and §Department of Chemistry, University of Cambridge, Lensfield Road, Cambridge CB2 1EW, United Kingdom

Communicated by Alexander Pines, University of California, Berkeley, CA, October 15, 2002 (received for review August 5, 2002)

The molecular conformation of peptide fragment 105–115 of transthyretin, TTR(105–115), previously shown to form amyloid fibrils *in vitro*, has been determined by magic-angle spinning solid-state NMR spectroscopy. ^{13}C and ^{15}N linewidth measurements indicate that TTR(105–115) forms a highly ordered structure with each amino acid in a unique environment. 2D ^{13}C-^{13}C and ^{15}N-^{13}C-^{13}C chemical shift correlation experiments, performed on three fibril samples uniformly ^{13}C,^{15}N-labeled in consecutive stretches of 4 aa, allowed the complete sequence-specific backbone and side-chain ^{13}C and ^{15}N resonance assignments to be obtained for residues 105–114. Analysis of the ^{15}N, ^{13}CO, $^{13}C^{\alpha}$, and $^{13}C^{\beta}$ chemical shifts allowed quantitative predictions to be made for the backbone torsion angles ϕ and ψ. Furthermore, four backbone ^{13}C–^{15}N distances were determined in two selectively ^{13}C,^{15}N-labeled fibril samples by using rotational-echo double-resonance NMR. The results show that TTR(105–115) adopts an extended β-strand conformation that is similar to that found in the native protein except for substantial differences in the vicinity of the proline residue.

Amyloid fibrils are highly organized aggregates formed by peptides and proteins with a wide variety of structures and functions. Fibril formation is associated with a number of protein deposition diseases including Alzheimer's disease, type II diabetes, and the transmissible spongiform encephalopathies (1, 2). In addition, many peptides and proteins not directly associated with disease have the propensity to self-assemble into amyloid fibrils *in vitro* (3, 4). Although fibrils are formed by polypeptides with different amino acid sequences and lengths, they share a number of common characteristics. They exhibit similar morphologies under electron microscopy and a characteristic ''cross-β'' pattern in x-ray fiber diffraction experiments (1, 2). The latter has been attributed to an extensive β-sheet structure in which the peptide strands are oriented perpendicular to the long fibril axis. The fibrils are assembled from a large number of molecules but do not form single crystals. Therefore, they are not amenable to characterization with solution-state NMR or x-ray crystallography. Solid-state NMR (SSNMR) spectroscopy, however, can be used to obtain site-specific structural information at atomic resolution in noncrystalline biological solids such as amyloid fibrils. Indeed, recent developments in SSNMR instrumentation and methodology (5) have enabled a number of structural details to be determined for various peptide fragments of the Alzheimer's β-peptide, ranging from 7 to 40 residues in length (6–9), for a peptide fragment of the human islet amyloid polypeptide (10), and for several peptides derived from prion proteins (11, 12).

In this article we describe the complete resonance assignments and determine the molecular conformation of a peptide fragment of transthyretin (TTR) in an amyloid fibril by using magic-angle spinning (MAS) SSNMR spectroscopy. TTR is a 55-kDa protein involved in the transport of thyroxine and retinol in plasma. The native protein is a homotetramer of 127-residue subunits and has extensive β-sheet structure (13). WT TTR forms amyloid fibrils *in vivo* in a condition termed senile systemic amyloidosis (14), and a number of naturally occurring TTR variants are associated with familial amyloid polyneuropathy (15). Full-length TTR (16), TTR variants (17, 18), and two 11-residue peptide fragments derived from the native sequence (16) have been shown readily to form amyloid fibrils *in vitro*. They are therefore important systems for the detailed investigations of the structure of amyloid fibrils and the mechanism of fibril formation (19). The peptides TTR(10–20) and TTR(105–115) correspond to the sequences that are found as β-strands A and G, respectively, in the native protein. Both strands are located at the surface of the thyroxine-binding channel formed by the homotetramer (20). Oriented fibrils formed by TTR(10–20) and TTR(105–115) exhibit the characteristic cross-β x-ray fiber diffraction patterns (21). The monomeric peptides have been found to adopt essentially random conformations in aqueous solution (22).

In the present work we have used 1D and 2D MAS SSNMR to probe the molecular conformation of TTR(105–115) in the fibrillar state. ^{13}C and ^{15}N linewidth measurements indicate that the peptide forms highly ordered fibrils in which there is a single unique environment for each residue. We have established the complete sequence-specific backbone and side-chain ^{13}C and ^{15}N resonance assignments for residues 105–114 in fibrils prepared from peptides uniformly ^{13}C,^{15}N (U-^{13}C,^{15}N) labeled in consecutive stretches of 4 aa. The 2D ^{13}C-^{13}C and ^{15}N-^{13}C-^{13}C chemical shift correlation techniques used here are analogous to those used recently to assign several (U-^{13}C,^{15}N)-labeled peptides and proteins (8, 23–27), and the complete resonance assignments represent the initial step in the determination of a high-resolution NMR structure for TTR(105–115) fibrils. The ^{15}N, ^{13}CO, $^{13}C^{\alpha}$, and $^{13}C^{\beta}$ chemical shifts have been used to predict the backbone torsion angles ϕ and ψ. Furthermore, we have measured four backbone ^{13}C–^{15}N distances in the 4- to 5-Å regime in two selectively ^{13}C,^{15}N-labeled fibril samples by using rotational-echo double resonance (REDOR) NMR (see below). The data indicate that the TTR(105–115) fibrils are extremely well ordered and that the fibrils represent an array of identical peptide molecules, each of which is in a fully extended β-strand conformation.

Methods

Preparation of Amyloid Fibrils. TTR(105–115) (YTIAALLSPYS) peptides for the resonance assignment experiments were synthesized by using standard solid-phase methods and purified by HPLC (CS Bio, San Carlos, CA). The peptides used for the REDOR measurements were synthesized by Midwest Biotech (Fishers, IN) and the Massachusetts Institute of Technology Cancer Center Biopolymers Facility. All ^{13}C,^{15}N-labeled, protected amino acids used in the peptide synthesis were purchased directly from Cambridge Isotope Laboratories (Andover, MA), with the exception of *N*-fluorenylmethoxycarbonyl,*O*-*t*-butyl

Abbreviations: SSNMR, solid-state NMR; MAS, magic-angle spinning; TTR, transthyretin; REDOR, rotational-echo double-resonance; CP, cross-polarization.

‡To whom correspondence may be addressed. E-mail: cem48@cam.ac.uk or rgg@mit.edu.

105 115

$TTR(105\text{-}115)_{YTIA}$: YTIAALLSPYS

$TTR(105\text{-}115)_{AALL}$: YTIAALLSPYS

$TTR(105\text{-}115)_{LSPY}$: YTIAALLSPYS

Fig. 1. Amino acid sequence of TTR(105–115) and labeling scheme used for the resonance assignments experiments. (U-^{13}C,^{15}N)-labeled residues are underlined.

ether-protected (U-^{13}C,^{15}N)threonine, (U-^{13}C,^{15}N)serine, (1-^{13}C)serine, (2-^{13}C)serine, and (^{15}N)tyrosine, which were synthesized by Midwest Biotech starting with isotopically labeled amino acids from Cambridge Isotope Laboratories.

Three TTR(105–115) fibril samples were used for all resonance assignment experiments. The peptides contained four (U-^{13}C,^{15}N)-labeled amino acids at positions 105–108, 108–111, and 111–114; these samples are referred to as $TTR(105\text{–}115)_{YTIA}$, $TTR(105\text{–}115)_{AALL}$, and $TTR(105\text{–}115)_{LSPY}$, respectively (Fig. 1). Note that the C-terminal residue (S115) was not (U-^{13}C,^{15}N) labeled because of the expense associated with the coupling of that residue to the resin with high yield. Two additional TTR(105–115) samples containing selectively ^{13}C,^{15}N-labeled amino acids were used for REDOR ^{13}C-^{15}N distance measurements. The first sample contained the ^{13}C and ^{15}N labels at the A108 ^{13}CO, L111 ^{13}C$^{\alpha}$, and L110 ^{15}N positions, and the second sample was labeled at S112 ^{13}CO, S115 ^{13}C$^{\alpha}$, and Y114 ^{15}N.

Amyloid fibrils were prepared by dissolving TTR(105–115) in a 10% acetonitrile/water solution (adjusted to pH 2 with HCl) at ≈15 mg/ml. The samples were incubated for 2 days at 37°C followed by incubation for 14 days at room temperature. The samples were routinely characterized by transmission electron microscopy. After this period the clear, viscous gel containing the fibrils was transferred to a centrifuge tube and washed twice with ≈2 ml of 10% acetonitrile/water at pH 2. After each wash the sample was centrifuged for 2 h at 4°C and ≈320,000 × *g*. After the second spin the pellet containing ≈10 mg of fibrils was packed into a 4-mm zirconia NMR rotor (Varian-Chemagnetics, Fort Collins, CO). The top of the rotor was sealed with epoxy to prevent dehydration during the MAS NMR experiments.

NMR Experiments. NMR experiments were performed on a custom-designed spectrometer (courtesy of D. J. Ruben, Francis Bitter Magnet Laboratory, Massachusetts Institute of Technology) operating at the frequencies of 500 MHz for ^{1}H, 125.7 MHz for ^{13}C, and 50.7 MHz for ^{15}N, by using a Varian-Chemagnetics 500-MHz triple-resonance T3 probe equipped with a 4-mm spinner module. Spinning frequencies of ≈9–11 kHz were used in all experiments and regulated to ±5 Hz with a Doty Scientific (Columbia, SC) spinning frequency controller, and the sample temperature was maintained at 2°C by using a stream of cooled nitrogen gas.

The 1D ^{13}C and ^{15}N MAS spectra were recorded with ramped cross-polarization (CP) (28, 29). The ^{1}H radio frequency field was set to 50 kHz, the ^{13}C field was ramped linearly through the $n = -1$ Hartmann-Hahn matching condition (between 38 and 42 kHz), and the contact time was 2 ms.

The 2D ^{13}C-^{13}C proton-driven spin diffusion experiments (30) used 5-μs 90° ^{13}C pulses and a 10-ms spin diffusion period. A ^{1}H radio frequency field matching the $n = 1$ rotary resonance condition (31) was applied during the mixing period to facilitate efficient ^{13}C-^{13}C magnetization transfer.

The 2D ^{15}N-^{13}C-^{13}C spectra were recorded by using the NCOCX and NCACX pulse sequences as described (26, 27). After ^{1}H-^{15}N CP and ^{15}N chemical shift evolution period (t_1), band-selective specific ramped CP (32) was used to transfer the

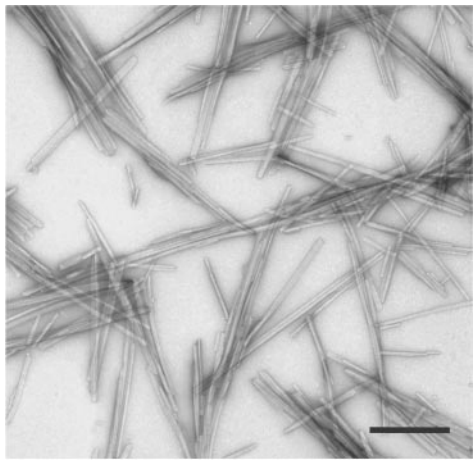

Fig. 2. Electron micrograph of TTR(105–115) fibrils. Amyloid fibrils were diluted to 100–200 μg/ml and negatively stained by using 2% (wt/vol) uranyl acetate. Fibrils were viewed in a Jeol 1200EX transmission electron microscope, using an accelerating voltage of 80 kV. (Scale bar: 200 nm.)

^{15}N magnetization selectively to ^{13}CO or ^{13}C$^{\alpha}$ by placing the ^{13}C carrier frequency ≈10–15 ppm outside the CO (for N → CO transfer) and C$^{\alpha}$ (for N → C$^{\alpha}$ transfer) regions. The ^{15}N radio frequency field strength was ≈35 kHz, the ^{13}C field was ramped linearly between ≈1 kHz below and ≈1 kHz above the $n = -1$ Hartmann–Hahn matching condition, and the mixing time was 3 ms. Immediately after the ^{15}N-^{13}C CP, a 10- to 20-ms ^{1}H-driven ^{13}C-^{13}C spin diffusion period was used to establish the intraresidue ^{13}C-^{13}C correlations.

Backbone ^{13}C-^{15}N distances were measured by using the REDOR experiment (33). The initial ^{13}C magnetization created via CP was observed as a spin-echo and dephased during the REDOR mixing period by using a train of rotor-synchronized 180° ^{15}N pulses. For each REDOR curve, S, a reference curve, S_0, was recorded in the absence of ^{15}N pulses to account for relaxation effects. The internuclear ^{13}C-^{15}N distances were extracted by fitting the quantity S/S_0 as a function of the REDOR mixing time to the analytical expression describing the dipolar dephasing.

During ^{15}N-^{13}C CP and REDOR mixing, 100-kHz continuous wave proton decoupling was used, and 70- to 80-kHz two pulse phase modulation decoupling (34) was used during all chemical shift evolution periods.

Results and Discussion

An electron micrograph of the fibrils formed by TTR(105–115) is shown in Fig. 2. The fibrils have variable lengths, are ≈10 nm wide, and are similar in appearance to those observed in disease-associated systems (1, 2).

The 1D ^{13}C and ^{15}N MAS spectra of (U-^{13}C,^{15}N)-labeled TTR(105–115) fibrils (Fig. 3) are extremely well resolved, with virtually all sites giving rise to narrow, single resonances. The spectral assignments indicated in Fig. 3 and listed in Table 1 were established by using 2D ^{13}C-^{13}C and ^{15}N-^{13}C-^{13}C correlation techniques, which are discussed in detail below. Widths at half height of ≈0.6–1.8 ppm and 0.7–1.5 ppm were observed for ^{13}C and ^{15}N resonances, respectively, with the majority of sites having linewidths of <1.0 ppm for ^{13}C and <1.3 ppm for ^{15}N (Table 4, which is published as supporting information on the PNAS web site, www.pnas.org). The ^{13}C and ^{15}N resonances in TTR(105–115) fibrils are significantly narrower than those characteristic of amorphous or disordered systems, and the linewidths compare favorably with those observed in (U-^{13}C,^{15}N)-labeled microcrystalline amino acids and peptides (23, 24). This

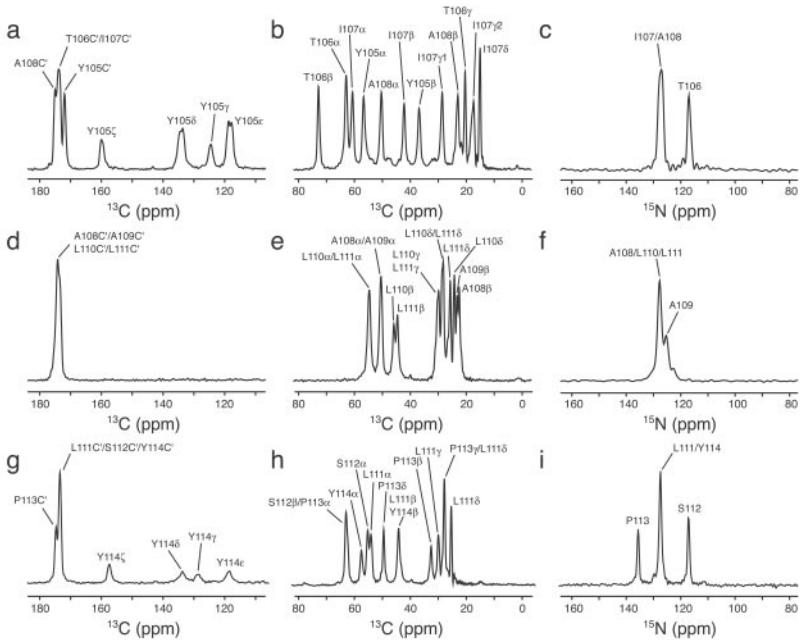

Fig. 3. 1D ^{13}C and ^{15}N MAS NMR spectra of (U-^{13}C,^{15}N)-labeled TTR(105–115) fibrils. ^{13}C carbonyl and aromatic (*a*, *d*, and *g*), ^{13}C aliphatic (*b*, *e*, and *h*), and ^{15}N amide (*c*, *f*, and *i*) spectral regions are shown for the $TTR(105–115)_{YTIA}$ (*a–c*), $TTR(105–115)_{AALL}$ (*d–f*), and $TTR(105–115)_{LSPY}$ (*g–i*) samples. ^{13}C and ^{15}N spectra were acquired by using the ramped CP pulse sequence (see text) with 128 and 512 scans, respectively, a 3-s recycle delay, and spinning frequencies of 8.929 kHz (*a–c*), 10.87 kHz (*d–f*), and 10.0 kHz (*g–i*).

finding implies that the inhomogeneous line broadening caused by disorder is minimal. This observation is remarkable given the fact that the fibrils are noncrystalline and indicates on the atomic level a highly ordered fibrillar structure with a narrow distribution of peptide conformations. The ^{13}C and ^{15}N chemical shift anisotropies and ^{1}H-^{13}C, ^{1}H-^{15}N, and ^{13}C-^{15}N dipolar interactions involving backbone resonances measured in TTR(105–115) fibrils (unpublished data) correspond to the rigid limit values and indicate the absence of appreciable dynamics along the peptide backbone.

Representative 2D ^{13}C-^{13}C and ^{15}N-^{13}C-^{13}C correlation spectra used to establish the sequence-specific backbone and side-chain ^{13}C and ^{15}N resonance assignments are shown in Figs. 4 and 5 for the $TTR(105–115)_{YTIA}$ sample. The complete set of 2D spectra is provided in Figs. 9 and 10, which are published as supporting information on the PNAS web site. The 2D ^{13}C-^{13}C experiments (Fig. 4) used proton-driven spin diffusion to establish the intraresidue ^{13}C-^{13}C correlations and identify amino acid types. In the aliphatic regions of the 2D spectra most cross-peaks corresponding to the one-bond correlations (indicated by dotted lines in Fig. 4) are well resolved, which enables the straightforward identification of the cross-peak patterns for all residues. A number of correlations with increasingly weaker intensities extending over two or more bonds and corresponding to multiple relayed one-bond transfers are also observed. Most remarkable is the fact that for $TTR(105–115)_{AALL}$ (Fig. 9), where two alanine and two leucine residues are (U-^{13}C,^{15}N) labeled, the C^{α}-C^{β}, C^{β}-C^{γ}, and C^{γ}-C^{δ} correlations for each residue can be readily identified, with the most significant overlap occurring in the Leu C^{δ} region.

The ^{15}N resonances were assigned by using 2D NCACX experiments (Fig. 5*b*), which establish the intraresidue ^{15}N-^{13}C correlations. All N-C^{α} correlations except Leu-110 and Leu-111 (Fig. 10) are well resolved in the 2D spectra and enable the unambiguous assignment of the amide ^{15}N resonances (Leu-110 and Leu-111 ^{15}N chemical shifts were obtained from N-C^{β} correlations generated by using ^{13}C-^{13}C proton-driven spin diffusion). 2D NCOCX experiments (Fig. 5*a*) were used to

Table 1. ^{13}C and ^{15}N chemical shifts measured in TTR(105–115) fibrils

Residue	^{15}N	^{13}CO	$^{13}C^{\alpha}$	$^{13}C^{\beta}$	$^{13}C^{\gamma}$	$^{13}C^{\delta}$	$^{13}C^{\varepsilon}$	$^{13}C^{\zeta}$
Y105	39.2	172.0	56.3	36.5	124.5	134.5/133.4	118.7/117.8	160.0
T106	117.0	173.5	62.6	72.5	20.0	—	—	—
I107	127.0	174.1	60.2	41.8	28.2/17.0	14.6	—	—
A108	128.0	174.5	49.9	22.1	—	—	—	—
A109	125.1	173.3	50.3	22.9	—	—	—	—
L110	127.0	174.2	54.4	45.5	29.4	28.2/23.9	—	—
L111	127.5	173.9	54.1	44.3	29.9	27.7/25.3	—	—
S112	117.2	173.6	55.4	63.2	—	—	—	—
P113	135.8	174.8	62.6	32.6	28.0	49.6	—	—
Y114	127.3	173.6	57.7	43.8	128.7	133.6	118.3	157.4
S115	—	—	57.8*	—	—	—	—	—

All chemical shifts are in ppm, referenced indirectly to the methyl ^{1}H resonance of 2,2-dimethylsilapentane-5-sulfonic acid (DSS) (35).
*S115 $^{13}C^{\alpha}$ chemical shift was measured in a selectively labeled fibril sample.

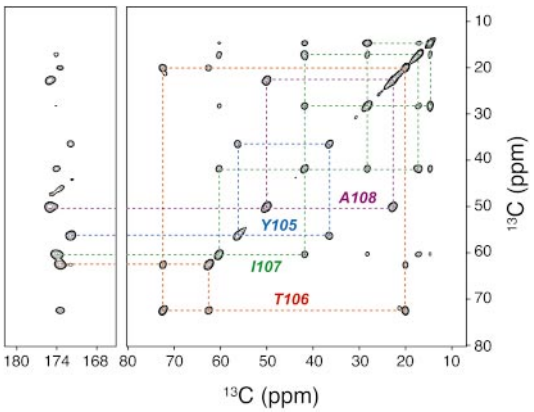

Fig. 4. 2D ^{13}C-^{13}C correlation spectrum of TTR(105–115)$_{YTIA}$ fibrils. The data were acquired at the spinning frequency of 8.929 kHz by using the proton-driven spin diffusion pulse sequence with a 10-ms ^{13}C-^{13}C mixing time (see text). The 2D data set was acquired according to Ruben and coworkers (36), with 200 complex points in the indirect dimension and the increment of 40 μs, resulting in the total t_1 evolution time of 8 ms. Sixty-four transients were averaged per point with a 3-s recycle delay, resulting in the total 2D acquisition time of ≈22 h. The intraresidue one-bond correlations are indicated by colored dotted lines as follows: Y105, blue; T106, red; I107, green; and A108, indigo.

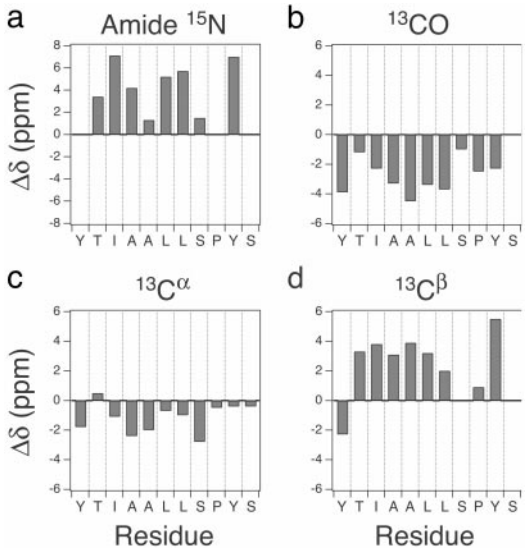

Fig. 6. Secondary ^{15}N and ^{13}C chemical shifts in TTR(105–115) fibrils. The secondary shifts (Δδ) for amide ^{15}N (*a*), ^{13}C carbonyl (*b*), $^{13}C^{\alpha}$ (*c*), and $^{13}C^{\beta}$ (*d*) resonances were calculated as $\Delta\delta = \delta_{EXP} - \delta_{RC}$, where δ_{EXP} and δ_{RC} are the experimentally observed and random coil chemical shifts in ppm, respectively. The random coil shifts correspond to the values used by the TALOS program (39) to provide quantitative predictions for the torsion angles ϕ and ψ (compare Table 2). The secondary shifts for Y105 ^{15}N, S115 ^{15}N, S115 ^{13}CO, and S115 $^{13}C^{\beta}$ could not be calculated; Y105 is the N-terminal residue and S115 was not (U-^{13}C,^{15}N) labeled in any of the samples (S115 $^{13}C^{\alpha}$ chemical shift was obtained by using a selectively labeled sample).

establish the interresidue correlations (between the ^{15}N resonance of residue *i* and ^{13}C resonances of residue *i*-1) required for sequence-specific assignments. Note that because of the isotope labeling scheme used, the sequence-specific ^{13}C and ^{15}N assignments for the TTR(105–115)$_{YTIA}$ and TTR(105–115)$_{LSPY}$ samples would be obtained by using only the 2D ^{13}C-^{13}C and NCACX experiments, whereas all three experiments are necessary to assign the spectra of TTR(105–115)$_{AALL}$ fibrils. Furthermore, we note that although three (U-^{13}C,^{15}N)-labeled TTR(105–115) fibril samples were used to assign the ^{13}C and ^{15}N chemical shifts in this work, inspection of the 2D correlation spectra indicates that complete sequence-specific resonance assignments could be established by using a single uniformly isotope-labeled fibril sample.

Site-specific ^{1}H, ^{13}C, and ^{15}N resonance assignments are in themselves a source of valuable structural information in solution-NMR and SSNMR studies of peptides and proteins because the secondary shifts (i.e., differences between the experimentally observed isotropic chemical shifts and the corresponding random coil values) can be used reliably to predict the conformation of the protein backbone (37–39). Fig. 6 shows the ^{13}CO, $^{13}C^{\alpha}$, $^{13}C^{\beta}$, and ^{15}N secondary shifts for the TTR(105–115) fibrils, which strongly indicate that the peptide adopts a β-strand conformation in the fibrillar state.

Quantitative predictions for backbone torsion angles ϕ and ψ in TTR(105–115) fibrils were made by using the TALOS program (39) (Table 2). Satisfactory convergence is obtained for eight of the nine residues, for which the program can predict ϕ and ψ. The torsion angles with estimated uncertainties of approximately ±20° are all between ≈−80° and −130° for ϕ and ≈125° and 145° for ψ. These angles are in the β-strand region of the Ramachandran plot. The conformation of the peptide bond between S112 and P113 could, in addition, be determined from the chemical shift data. The difference of 4.6 ppm between the $^{13}C^{\beta}$ and $^{13}C^{\gamma}$ chemical shifts for Pro-113 in TTR(105–115) fibrils indicates that the S112-P113 peptide bond exists in a trans conformation (40). This conformation is the more common one in peptides and globular proteins, and indeed the S112-P113 peptide bond in native TTR is trans (13).

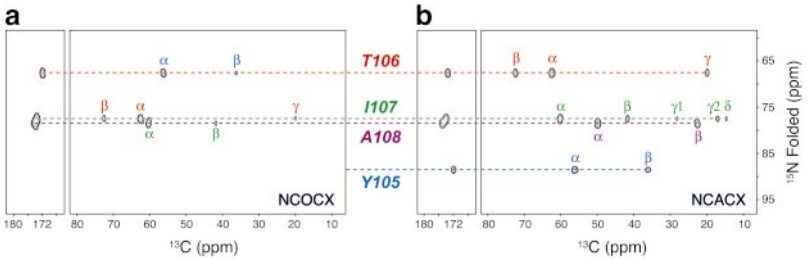

Fig. 5. 2D ^{15}N-^{13}C-^{13}C correlation spectra of TTR(105–115)$_{YTIA}$ fibrils. The NCOCX spectrum (*a*) correlates the $^{15}N_i$ and $^{13}C_{i-1}$ resonances, and the NCACX spectrum (*b*) correlates the $^{15}N_i$ and $^{13}C_i$ resonances. The data were acquired by using the NCOCX and NCACX pulse sequences (see text), with a 3-ms ^{15}N-^{13}CO or ^{15}N-C$^{\alpha}$ band-selective CP transfer followed by a 10-ms ^{1}H-driven spin-diffusion ^{13}C-^{13}C mixing, and the spinning frequency of 8.929 kHz. The 2D data set was acquired according to Ruben and coworkers (36), with 21 complex points in the indirect dimension and the increment of 0.4 ms, resulting in the total t_1 evolution time of 8 ms. A total of 256 transients were averaged per point and a 3-s recycle delay was used, resulting in the total 2D acquisition time of ≈10 h. The residues participating in the ^{15}N-^{13}C correlations are labeled as follows: Y105, blue; T106, red; I107, green; and A108, indigo.

Table 2. Backbone torsion angles ϕ and ψ in TTR(105–115) fibrils and WT TTR

Residue	Predicted TALOS ϕ angle in fibrils, °	Predicted TALOS ψ angle in fibrils, °	x-ray ϕ angle in WT TTR, °‡	x-ray ψ angle in WT TTR, °‡
Y105	—*	—*	−117/−116	127/129
T106	—†	—†	−120/−124	115/114
I107	−125 ± 20	143 ± 12	−105/−102	119/126
A108	−117 ± 22	133 ± 13	−104/−112	138/147
A109	−131 ± 14	129 ± 18	−126/−140	141/131
L110	−112 ± 18	120 ± 16	−124/−112	111/113
L111	−118 ± 22	137 ± 15	−99/−98	145/132
S112	−109 ± 22	136 ± 27	−140/−130	160/161
P113	−81 ± 31	126 ± 19	−50/−61	−49/−40
Y114	−112 ± 27	138 ± 15	−113/−115	20/14
S115	—*	—*	−155/−156	149/147

Backbone torsion angles obtained for TTR(105–115) fibrils by using TALOS (39) are compared with the corresponding angles in WT TTR (13). TALOS uses experimental ^{13}C and ^{15}N chemical shifts (compare Table 1) and sequence homology to predict the most likely values for ϕ and ψ.

*Torsion angles for the N- and C-terminal residues are not accessible (39).

†No satisfactory convergence was obtained for T106.

‡Entries correspond to the two subunits of the crystallographic dimer (13).

Table 3. Backbone carbon-nitrogen distances in TTR(105–115) fibrils and WT TTR

Atoms		Measured REDOR distance in fibrils, Å*	Predicted TALOS distance in fibrils, Å	x-ray distance in WT TTR, Å†
A108 CO	L110 N	4.25 ± 0.15	4.28	4.34/4.36
L111 C^{α}	L110 N	4.56 ± 0.12	4.60	4.54/4.56
S112 CO	Y114 N	4.06 ± 0.06	3.94	3.26/3.29
S115 C^{α}	Y114 N	$5.0^{+1.5}_{-0.5}$	4.80	4.11/4.17

Distances measured in selectively ^{13}C, ^{15}N-labeled fibrils by using REDOR (33) are compared with the corresponding distances in a TTR(105–115) backbone model constructed according to the TALOS (39) predictions for ϕ and ψ (compare Table 2) and in the WT TTR x-ray structure (13).

*REDOR dephasing data were analyzed by using a two-spin model (see text) and the uncertainties correspond to the 95% confidence limit.

†Entries correspond to the two subunits of the crystallographic dimer (13).

We next performed REDOR experiments (33) on selectively ^{13}C,^{15}N-labeled TTR(105–115) fibrils to determine several carbon-nitrogen distances along the peptide backbone (Fig. 7). The measured distances (Table 3) are in good agreement (within ≈0.05–0.2 Å) with those found in a TTR(105–115) backbone model constructed by using the ϕ and ψ angles obtained from TALOS (see below). Furthermore, the distances in the central region of the peptide (A108 CO-L110 N and L111 C^{α}-L110 N) are consistent with the WT TTR x-ray structure (13), whereas the S112 CO-Y114 N and S115 C^{α}-Y114 N distances in the fibril are significantly longer than the corresponding distances in native TTR(13). Despite the potential presence of non-negligible intermolecular dipolar couplings a simple two-spin model was used to analyze the REDOR dephasing data. The rationale for this decision is that no information is available about the supramolecular organization of peptides in the fibril, and hence about the magnitude of the intermolecular couplings. The influence of these couplings on the dipolar dephasing was investigated via simulations of multiple spin systems resulting from canonical in-register parallel and antiparallel β-strand topologies. For the parallel arrangement we found that the intramolecular distances obtained by using the two-spin model are underestimated by ≈0.1–0.3 Å. For the antiparallel arrangement the L111 C^{α}-L110N distance is underestimated by ≈0.5 Å, and all other measurements are unaffected. In summary, the use of the two-spin model does not lead to significant systematic errors for most of the intramolecular distances measured, regardless of the arrangement of the peptides in the fibril, and it does not alter the conclusion that TTR(105–115) adopts an extended β-strand conformation in the fibril.

Fig. 8 compares the structure of the peptide fragment corresponding to residues 105–115 in WT TTR(13) and the backbone model for TTR(105–115) in the fibrillar state constructed by using the torsion angles in Table 2. In WT TTR residues 105–111 have typical β-strand ϕ and ψ angles and residues 112–114 form a turn, with Pro-113 torsion angles in the helical region of the

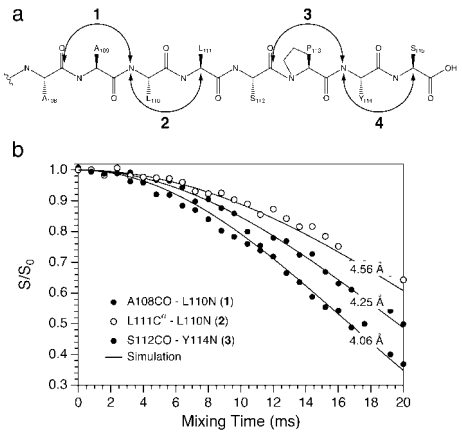

Fig. 7. Backbone ^{13}C-^{15}N distances measured in selectively labeled TTR(105–115) fibrils by using REDOR. The schematic of the peptide backbone and the specific distances measured are shown (*a*). Distances indicated in *a* as 1 and 2 were measured in fibrils isotopically labeled at A108 ^{13}CO, L111 $^{13}C^{\alpha}$, and L110 ^{15}N and distances indicated as 3 and 4 were measured in fibrils labeled at S112 ^{13}CO, S115 $^{13}C^{\alpha}$, and Y114 ^{15}N. Experimental (circles) and simulated (lines) REDOR S/S_0 curves are shown (*b*). The experimental curves correspond to the distances: A108 CO-L110 N (◎), L111 C^{α}-L110 N (○), and S112 CO-Y114 N (●). The measured distances are indicated in *b* and summarized in Table 3 (the S115 C^{α}-Y114 N measurement was omitted for clarity). Spectra were acquired with 320–384 transients and the spinning frequency of 10.0 kHz ± 5 Hz.

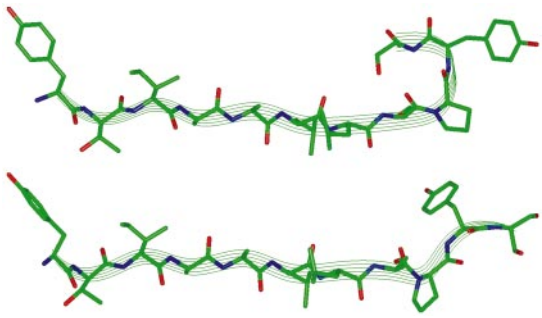

Fig. 8. X-ray structure of the peptide fragment corresponding to residues 105–115 in WT TTR (13) (*Upper*) and the backbone model for the TTR(105–115) peptide in the fibrillar state constructed by using the ϕ and ψ angles in Table 2 (*Lower*). The Y105 and T106 backbone torsion angles used in the model were obtained from SSNMR measurements of internuclear distances and torsion angles (unpublished data) analogous to those published in refs. 41–44. No constraints are available for ψ_{S115} and the experiments designed to probe side-chain χ angles are currently in progress (unpublished data). These moieties are present for illustration purposes only and their conformations in the model correspond to those found in WT TTR (13). The figure was prepared by using the program INSIGHT II version 2000 (Accelerys, San Diego).

Ramachandran plot (Table 2). The comparison of torsion angles and distances for WT TTR and TTR(105–115) peptide in the fibrils reveals remarkable similarity in the backbone conformation of residues 107–111. However, the backbone turn involving residues 112–114, characterized in WT TTR (13) by the relatively short S112 CO-Y114 N distance (Table 3), is absent in TTR(105–115) fibrils where we find typical β-strand ϕ and ψ values for residues 112–114. In the native structure, Pro-113 promotes interactions with adjacent strands and dictates tertiary contacts, preventing self-association. In the absence of this greater context, and despite its inability to participate in a hydrogen-bonding network, the proline is instead fully incorporated into the β-strand and possibly also into the β-sheet fibrillar array. This observation illustrates the importance of 3D context in the adoption of secondary structure and also represents one way in which nature appears to have neatly manipulated folding propensity to prevent aggregation.

Conclusions

We have carried out a set of experiments required for the determination of the complete atomic-resolution structure of an amyloid fibril, by characterizing the molecular conformation of a peptide fragment of transthyretin with 1D and 2D ^{13}C and ^{15}N MAS NMR techniques. The present results show that exceptionally high-quality NMR data can be obtained for amyloid fibrils. The ^{13}C and ^{15}N linewidth measurements indicate that TTR(105–115) forms a highly ordered structure with each amino acid in a unique environment. This observation is consistent with the concept that the amyloid core structure is generic and can override the properties of individual sequences that define the structures of globular proteins (19, 45). Quantitative predictions for the backbone torsion angles were obtained by using the sequence specific ^{13}C and ^{15}N backbone and side-chain chemical shifts. Furthermore, four backbone ^{13}C–^{15}N distances in the 4- to 5-Å range were measured by using REDOR NMR. The results indicate that TTR(105–115) adopts a β-strand conformation in the fibrillar state in a structure remarkably similar to that found in the native protein, with the exception of the region surrounding the proline residue. Although we as yet have no information about the 3D organization of the peptides, the quality of the NMR data will enable us to probe the higher-order architecture and determine the complete structure of an amyloid fibril to atomic resolution.

We thank J. Zurdo, V. Bajaj, and M. McMahon for stimulating discussions. C.P.J. is a National Science Foundation Predoctoral Fellow. C.E.M. is a Royal Society Dorothy Hodgkin Research Fellow. N.S.A. is a National Institutes of Health Postdoctoral Fellow (1 F32 NS10964-01). The research of C.M.D. is supported in part by the Wellcome Trust, and the research of R.G.G. is supported by National Institutes of Health Grants GM-23403 and RR-00995.

1. Sunde, M. & Blake, C. C. F. (1998) *Q. Rev. Biophys.* **31,** 1–39.
2. Kelly, J. W. (1998) *Curr. Opin. Struct. Biol.* **8,** 101–106.
3. Guijarro, J. I., Sunde, M., Jones, J. A., Campbell, I. D. & Dobson, C. M. (1998) *Proc. Natl. Acad. Sci. USA* **95,** 4224–4228.
4. Chiti, F., Webster, P., Taddei, N., Clark, A., Stefani, M., Ramponi, G. & Dobson, C. M. (1999) *Proc. Natl. Acad. Sci. USA* **96,** 3590–3594.
5. Griffin, R. G. (1998) *Nat. Struct. Biol.* **5,** 508–512.
6. Lansbury, P. T., Costa, P. R., Griffiths, J. M., Simon, E. J., Auger, M., Halverson, K. J., Kocisko, D. A., Hendsch, Z. S., Ashburn, T. T., Spencer, R. G. S., *et al.* (1995) *Nat. Struct. Biol.* **2,** 990–998.
7. Benzinger, T. L. S., Gregory, D. M., Burkoth, T. S., Miller-Auer, H., Lynn, D. G., Botto, R. E. & Meredith, S. C. (1998) *Proc. Natl. Acad. Sci. USA* **95,** 13407–13412.
8. Balbach, J. J., Ishii, Y., Antzutkin, O. N., Leapman, R. D., Rizzo, N. W., Dyda, F., Reed, J. & Tycko, R. (2000) *Biochemistry* **39,** 13748–13759.
9. Antzutkin, O. N., Balbach, J. J., Leapman, R. D., Rizzo, N. W., Reed, J. & Tycko, R. (2000) *Proc. Natl. Acad. Sci. USA* **97,** 13045–13050.
10. Griffiths, J. M., Ashburn, T. T., Auger, M., Costa, P. R., Griffin, R. G. & Lansbury, P. T. (1995) *J. Am. Chem. Soc.* **117,** 3539–3546.
11. Heller, J., Kolbert, A. C., Larsen, R., Ernst, M., Bekker, T., Baldwin, M., Prusiner, S. B., Pines, A. & Wemmer, D. E. (1996) *Protein Sci.* **5,** 1655–1661.
12. Laws, D. D., Bitter, H.-M. L., Liu, K., Ball, H. L., Kaneko, K., Wille, H., Cohen, F. E., Prusiner, S. B., Pines, A. & Wemmer, D. E. (2001) *Proc. Natl. Acad. Sci. USA* **98,** 11686–11690.
13. Blake, C. C. F., Geisow, M. J., Oatley, S. J., Rerat, B. & Rerat, C. (1978) *J. Mol. Biol.* **121,** 339–356.
14. Westermark, P., Sletten, K., Johansson, B. & Cornwell, G. G. (1990) *Proc. Natl. Acad. Sci. USA* **87,** 2843–2845.
15. Saraiva, M. J. M. (2001) *Hum. Mutat.* **17,** 493–503.
16. Gustavsson, A., Engstrom, U. & Westermark, P. (1991) *Biochem. Biophys. Res. Commun.* **175,** 1159–1164.
17. Colon, W. & Kelly, J. W. (1992) *Biochemistry* **31,** 8654–8660.
18. Bonifacio, M. J., Sakaki, Y. & Saraiva, M. J. (1996) *Biochim. Biophys. Acta* **1316,** 35–42.
19. MacPhee, C. E. & Dobson, C. M. (2000) *J. Mol. Biol.* **297,** 1203–1215.
20. Blake, C. C. F. & Oatley, S. J. (1977) *Nature* **268,** 115–120.
21. Jarvis, J. A., Craik, D. J. & Wilce, M. C. J. (1993) *Biochem. Biophys. Res. Commun.* **192,** 991–998.
22. Jarvis, J. A., Kirkpatrick, A. & Craik, D. J. (1994) *Int. J. Peptide Protein Res.* **44,** 388–398.
23. Rienstra, C. M., Hohwy, M., Hong, M. & Griffin, R. G. (2000) *J. Am. Chem. Soc.* **122,** 10979–10990.
24. Detken, A., Hardy, E. H., Ernst, M., Kainosho, M., Kawakami, T., Aimoto, S. & Meier, B. H. (2001) *J. Biomol. NMR* **20,** 203–221.
25. McDermott, A., Polenova, T., Bockmann, A., Zilm, K. W., Paulsen, E. K., Martin, R. W. & Montelione, G. T. (2000) *J. Biomol. NMR* **16,** 209–219.
26. Egorova-Zachernyuk, T. A., Hollander, J., Fraser, N., Gast, P., Hoff, A. J., Cogdell, R., de Groot, H. J. M. & Baldus, M. (2001) *J. Biomol. NMR* **19,** 243–253.
27. Pauli, J., Baldus, M., van Rossum, B., de Groot, H. & Oschkinat, H. (2001) *Chembiochem* **2,** 272–281.
28. Pines, A., Gibby, M. G. & Waugh, J. S. (1973) *J. Chem. Phys.* **59,** 569–590.
29. Metz, G., Wu, X. & Smith, S. O. (1994) *J. Magn. Reson. A* **110,** 219–227.
30. Suter, D. & Ernst, R. R. (1985) *Phys. Rev. B* **32,** 5608–5627.
31. Oas, T. G., Griffin, R. G. & Levitt, M. H. (1988) *J. Chem. Phys.* **89,** 692–695.
32. Baldus, M., Petkova, A. T., Herzfeld, J. & Griffin, R. G. (1998) *Mol. Phys.* **95,** 1197–1207.
33. Gullion, T. & Schaefer, J. (1989) *Adv. Magn. Reson.* **13,** 57–83.
34. Bennett, A. E., Rienstra, C. M., Auger, M., Lakshmi, K. V. & Griffin, R. G. (1995) *J. Chem. Phys.* **103,** 6951–6957.
35. Wishart, D. S., Bigam, C. G., Yao, J., Abildgaard, F., Dyson, H. J., Oldfield, E., Markley, J. L. & Sykes, B. D. (1995) *J. Biomol. NMR* **6,** 135–140.
36. States, D. J., Haberkorn, R. A. & Ruben, D. J. (1982) *J. Magn. Reson.* **48,** 286–292.
37. Saito, H. (1986) *Magn. Reson. Chem.* **24,** 835–852.
38. Wishart, D. S. & Sykes, B. D. (1994) *Methods Enzymol.* **239,** 363–392.
39. Cornilescu, G., Delaglio, F. & Bax, A. (1999) *J. Biomol. NMR* **13,** 289–302.
40. Sarkar, S. K., Torchia, D. A., Kopple, K. D. & VanderHart, D. L. (1984) *J. Am. Chem. Soc.* **106,** 3328–3331.
41. Jaroniec, C. P., Tounge, B. A., Herzfeld, J. & Griffin, R. G. (2001) *J. Am. Chem. Soc.* **123,** 3507–3519.
42. Jaroniec, C. P., Filip, C. & Griffin, R. G. (2002) *J. Am. Chem. Soc.* **124,** 10728–10742.
43. Rienstra, C. M., Hohwy, M., Mueller, L. J., Jaroniec, C. P., Reif, B. & Griffin, R. G. (2002) *J. Am. Chem. Soc.* **124,** 11908–11922.
44. Rienstra, C. M., Tucker-Kellogg, L., Jaroniec, C. P., Hohwy, M., Reif, B., Lozano-Perez, T., Tidor, B. & Griffin, R. G. (2002) *Proc. Natl. Acad. Sci. USA* **99,** 10260–10265.
45. Dobson, C. M. (2001) *Philos. Trans. R. Soc. London B* **356,** 133–145.

Supporting Information

Molecular Conformation of a Peptide Fragment of Transthyretin in an Amyloid Fibril

Christopher P. Jaroniec, Cait E. MacPhee, Nathan S. Astrof,
Christopher M. Dobson, Robert G. Griffin

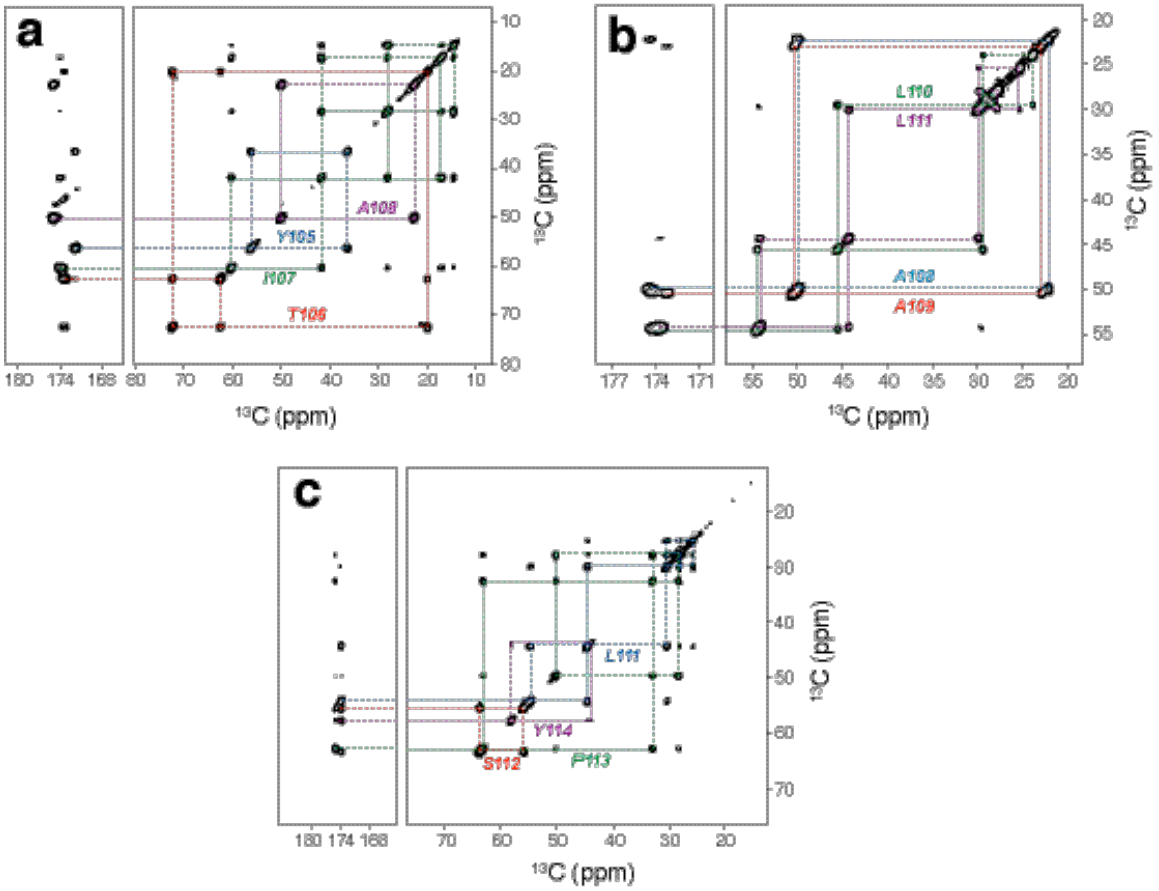

Figure S1. 2D ^{13}C-^{13}C correlation spectra of TTR(105-115)$_{YTIA}$ (a), TTR(105-115)$_{AALL}$ (b), and TTR(105-115)$_{LSPY}$ (c) fibrils. Spectra were acquired at the spinning frequencies of 8.929 kHz (a), 10.87 kHz (b), and 10.0 kHz (c), using the proton-driven spin diffusion pulse sequence (1) with a 10 ms ^{13}C-^{13}C mixing time (see text). 2D data sets were acquired according to Ruben and co-workers (2), with 100-250 complex points in the indirect dimension and increments of 40-92 □s, resulting in the total t_1 evolution times of 8-10 ms. 64 transients were averaged per point with a 3 s recycle delay, resulting in the total 2D acquisition times of ~11-27 h. The intraresidue one-bond correlations are indicated in the spectra by colored dotted lines as follows: (a) Y105 (blue), T106 (red), I107 (green), A108 (indigo); (b) A108 (blue), A109 (red), L110 (green), L111 (indigo); (c) L111 (blue), S112 (red), P113 (green), Y114 (indigo).

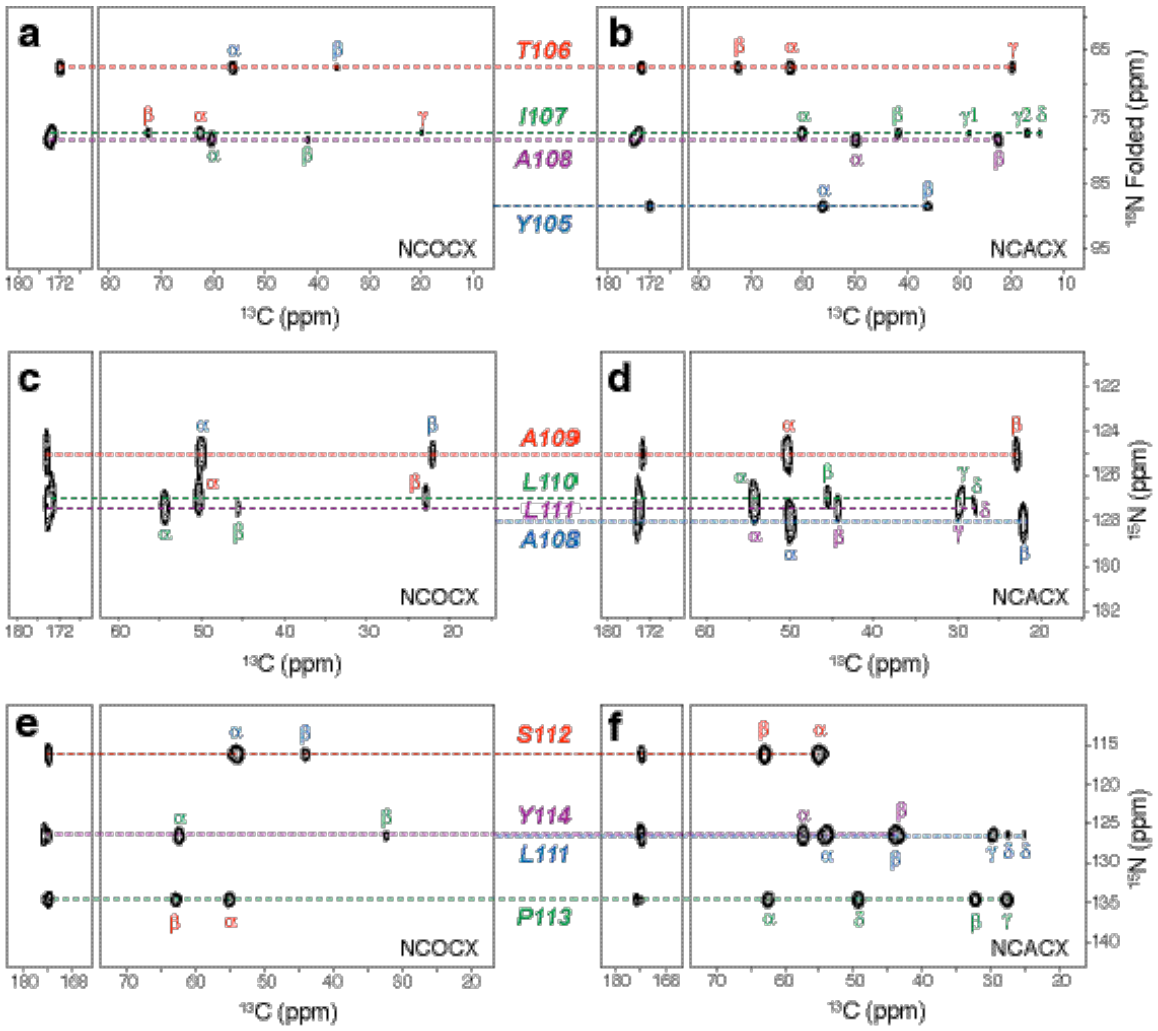

Figure S2. 2D ^{15}N-^{13}C-^{13}C correlation spectra of TTR(105-115)$_{YTIA}$ (a)-(b), TTR(105-115)$_{AALL}$ (c)-(d), and TTR(105-115)$_{LSPY}$ (e)-(f) fibrils. The NCOCX spectra (a), (c), (e) correlate the $^{15}N_i$ and $^{13}C_{i-1}$ resonances, and the NCACX spectra (b), (d), (f) correlate the $^{15}N_i$ and $^{13}C_i$ resonances. The spectra were acquired using the NCOCX and NCACX pulse sequences (3, 4), with a 3 ms ^{15}N-^{13}CO or ^{15}N-C□ band-selective CP transfer (5) followed by a 10-20 ms ^{1}H-driven spin-diffusion ^{13}C-^{13}C mixing (see text), and the spinning frequencies of 8.929 kHz (a)-(b), 10.87 kHz (c)-(d), and 10.0 kHz (e)-(f). 2D data sets were acquired according to Ruben and co-workers (2), with 7-21 complex points in the indirect dimension and increments of 0.4-1.656 ms, resulting in the total t_1 evolution times of 8-12 ms. 256-768 transients were averaged per point and a 3 s recycle delay was used, resulting in the total 2D acquisition time of ~10 h. For each pair of NCOCX and NCACX spectra the residues participating in the ^{15}N-^{13}C correlations are labeled as follows: (a)-(b) Y105 (blue), T106 (red), I107 (green), A108 (indigo); (c)-(d) A108 (blue), A109 (red), L110 (green), L111 (indigo); (e)-(f) L111 (blue), S112 (red), P113 (green), Y114 (indigo).

Table S1. ^{13}C and ^{15}N linewidths measured in TTR(105-115) fibrils

Residue	^{15}N	^{13}CO	$^{13}C\alpha$	$^{13}C\beta$	$^{13}C\gamma$	$^{13}C\delta$	$^{13}C\varepsilon$	$^{13}C\zeta$
Y105	0.73	0.87	1.11	1.11	1.50	—	—	1.45
T106	1.14	0.93	1.10	0.88	0.76	—	—	—
I107	1.48	0.94	1.10	1.02	1.03/1.48	0.70	—	—
A108	1.30	0.85	0.96	0.81	—	—	—	—
A109	1.34	0.85	0.94	0.87	—	—	—	—
L110	1.40	1.03	0.96	0.97	0.80	0.83/0.60	—	—
L111	1.02	1.01	1.04	0.86	0.85	0.58/0.60	—	—
S112	0.98	1.06	0.90	0.81	—	—	—	—
P113	0.91	0.92	0.98	0.88	0.82	0.76	—	—
Y114	1.30	0.98	1.07	1.86	1.74	—	—	1.33

Linewidths in ppm are obtained from 1D and 2D NMR spectra described in the text.

References

1. Suter, D. & Ernst, R. R. (1985) *Phys. Rev. B* **32,** 5608-5627.
2. States, D. J., Haberkorn, R. A. & Ruben, D. J. (1982) *J. Magn. Reson.* **48,** 286-292.
3. Egorova-Zachernyuk, T. A., Hollander, J., Fraser, N., Gast, P., Hoff, A. J., Cogdell, R., de Groot, H. J. M. & Baldus, M. (2001) *J. Biomol. NMR* **19,** 243-253.
4. Pauli, J., Baldus, M., van Rossum, B., de Groot, H. & Oschkinat, H. (2001) *ChemBiochem* **2,** 272-281.
5. Baldus, M., Petkova, A. T., Herzfeld, J. & Griffin, R. G. (1998) *Mol. Phys.* **95,** 1197-1207.